Computing and Informatics, Vol. 43, 2024, 1455–1482, doi: 10.31577/cai_2024_6_1455

MULTIPLE FEATURES EXTRACTION AND FUSION FOR ULTRASOUND DYNAMIC IMAGES CLASSIFICATION

Xiaojun Chen

School of Computer Science and Communication Engineering
Jiangsu University
Affiliated Hospital of Jiangsu University
Zhenjiang, China
e-mail: cxj@ujs.edu.cn

Jia Ke, Yaning Zhang

School of Management
Jiangsu University
Zhenjiang, China
e-mail: kejia@ujs.edu.cn, 2814301746@qq.com

Lu Liu

School of Computing and Mathematical Sciences
University of Leicester
Leicester, U.K.
e-mail: l.liu@leicester.ac.uk

Wenjing Lu

Affiliated Hospital of Jiangsu University
Zhenjiang, China
e-mail: 375516574@qq.com

Shenqi Jing, Xiaoliang Zhang

Jiangsu Province Hospital
Nanjing, China
e-mail: jingshenqi@njmu.edu.cn, 230229564@seu.edu.cn

Xinxin Guo

School of Management
Jiangsu University
Zhenjiang, China
e-mail: bzhmgx@163.com

Anna Shen

Affiliated Hospital of Jiangsu University
Zhenjiang, China
e-mail: annashen@ujs.edu.cn

Abstract. Ultrasound examination is of great significance in the clinical diagnosis of diseases. Processing and analyzing ultrasound images through artificial intelligence technology and providing assistance in decision-making has been a hot topic of research for several years. However, since most medical images exist in the form of pictures, the current processing methods for ultrasound images basically continue to adopt the technical achievements related to static medical image processing not considering the characteristics reflected by the dynamically changing ultrasound images thus resulting in a missed diagnosis of diseases. To this end, this paper proposes an innovative multi-feature extraction and fusion method for ultrasound dynamic image classification which first extracts various types of underlying features such as texture, edge, and shape of salient targets in medical images that apply to dynamic images. Then, the feature frequency-inverse image frequency (FF-IIF) multi-feature fusion algorithm is used to generate an adaptive combined feature classification. In the experiments, the effects of the proposed algorithm are verified for three ultrasound examination items respectively. The experimental results show that the features extracted by the multi-feature fusion algorithm using FF-IIF still maintain a certain degree of fault tolerance and stability under the dynamic changes of ultrasound probe position and orientation. The computation time of the algorithm is moderate and perfectly adapted to the real-time examination of ultrasound medicine.

Keywords: Ultrasound dynamic image, medical image features, video features, features extraction, features fusion, feature frequency-inverse image frequency

Mathematics Subject Classification 2010: 68-T45

1 INTRODUCTION

Medical Imaging (MI) refers to digital medical images and videos obtained by digital medical imaging devices or other equipment [1], including X-ray Radiography (X-Ray Radiography), Computed Tomography (CT), Magnetic Resonance Imaging (MRI), Pathological Image (PI), Endoscopy (EC), Ultrasound (US), etc. [2]. Unlike medical images such as X-ray Radiography, Computed Tomography, and MRI, ultrasound images are digital video files that display and store the echo values of sound waves in different tissues and organs of the body through digital medical devices [3]. In the same ultrasound examination, the doctor can collect the image information of several human tissues and organs such as liver, gallbladder, spleen and pancreas by moving the probe and detect the specific health condition of the tissues and organs from different positions and angles by tilting, rotating, arranging and pressing the probe [4]. For this reason, it is necessary to select features with high specificity and invariance to accurately describe the various tissues and organs of the human body in ultrasound dynamic images [5].

Image features are the basic semantic concepts formed by the human eye through the abstraction of intuitive feelings after the observation of images, and currently commonly used image features include color features, texture features, shape features, etc. [6]. Because ultrasound medical images are grayscale images, color features are generally not used. Texture features reflect the properties of the surface structure organization arrangement of the object surface with slow changes or periodic changes and are suitable for medical image processing. There are two types of representations of shape features, area features and contour features (edge features) [7]. The area feature mainly reflects the regularity of the change of the value of the pixel points in the internal area of the whole shape, with certain geometric characteristics, and has certain invariance in rotation, translation, and expansion, which is especially suitable for dynamic scenes [8]. Contour features are mainly concerned with the outer boundaries of the object, and contour features are those sets of pixels in the image where there are discontinuities in the distribution of features such as color (gray scale) and texture, and where there are step changes or roof-like changes in the characteristics around the image [9]. At present, more underlying features have been applied in medical image processing, but how to extract the representative underlying features in medical dynamic images is the focus of this paper [10].

After acquiring multiple features of medical images, it is necessary to generate adaptive combined feature components using multi-feature fusion algorithms, and currently algorithms such as Principal Component Analysis (PCA), Backward Feature Elimination (BFE), and Dynamic Causal Model (DCM) are commonly used to calculate effective combinations of feature components [11]. Several combination algorithms have been applied to combine the underlying features of medical images, but it is still challenging to select and combine the appropriate medical dynamic image feature components [12].

Aiming at the problems of extracting the representative underlying features of medical dynamic images and selecting and combining appropriate multi-feature components of medical dynamic images, this paper proposes a self-adaptive multi-feature fusion algorithms to select and combine various feature components to achieve effective classification of various human tissues and organs. The major contributions of the article are summarized as follows:

1. The current status of research on the underlying features of ultrasound organ characterization is analyzed, the characteristics of various underlying features are comprehensively compared, and calculation formulas for various representative features of self-adaptive combination and fusion methods are provided.
2. The FF-IIF algorithm was proposed to calculate the weight values of the underlying features of tissues and organs in medical examination projects. A threshold was used to filter out redundant or even useless underlying features, and the feature components and weight values were merged and provided to the classification module. The FF-IIF algorithm has a moderate computational time and is fully suitable for real-time ultrasound medical examination.
3. A multi-feature extraction and fusion method for ultrasound dynamic image classification is proposed which extracts the underlying features of prominent targets in medical images. This method maintains a certain degree of fault tolerance and stability in extracting features under dynamic changes in the position and direction of ultrasound probes.

The rest of the paper is organized as follows: Section 2 presents a review of related works, Section 3 introduces some techniques and methods of how to carry out the experiments, and results are displayed and visualized in Section 4. Section 5 summarizes the research process and prospects for future directions.

2 RELATED WORKS

2.1 The Underlying Characteristics of the Image

2.1.1 Texture Characteristics

The texture characteristics of different organs in ultrasound dynamic images have some variability, for example, the texture of the liver is smoother and can be seen as a stable brightness variation over the whole area, while the texture of the kidney is full of abrupt changes and can be seen as a brightness variation that contains some kind of repetitive streaking pattern. Specifically, Gray-level Co-occurrence Matrix (GLCM) and Tamura texture features are selected [13].

Grayscale co-occurrence matrix: The grayscale covariance matrix of the image is described by defining a second-order joint probability distribution, the main features of the grayscale co-occurrence matrix are Contrast, Autocorrelation, Dissimilarity, Energy, Entropy, Homogeneity, Variance, Sumvariance and Correlation coefficient.

Tamura texture features: Tamura texture feature is a property proposed in the psychological study of human visual perception of texture, and generally uses contrast, orientation, and roughness for texture feature recognition.

Rogers et al. used serialized computed tomography texture features to achieve an effective and accurate image classification function [14]. Feng et al. used the underlying features of bilateral texture filtering to achieve efficient and accurate computed tomography and MRI image fusion [15]. Santos et al. proposed a method based on a hybrid depth and texture feature space for classifying the minimal change disease (MCD) and glomerulosclerosis (GS) on pathological images [16]. Kawashima et al. designed a texture analysis algorithm to extract 33 texture features from ultrasound images, and 19 texture features were found to have good sensitivity and specificity for classifying malignant tumors by evaluation [17].

2.1.2 Invariant Moment Characteristics

Invariant moment functions are widely used in the fields of object representation, pattern recognition and image analysis because of their rotation, translation and expansion invariance. The lower order moments reflect the main overall information of the image, and the higher order moments reflect the detailed information of the image. The various invariant moments not only describe the global characteristics of the object shape in the image, but also provide a large amount of information about different geometric features of the object, such as size, position, orientation and shape. Since ultrasonography quickly switches between human organs by moving the probe, more stable geometric abstraction characteristics are generally used to describe its features. The description methods for target abstraction features based on regional features mainly include Hu Moments (HM), Polar Radius Moment (PRM), Complex Moment (CM), orthogonal invariant moments, and improved regional invariant moments proposed by Hu.

Li et al. used an improved adaptive moment estimation to optimize the conjugate gradient algorithm to efficiently achieve the reconstruction work on medical images [18]. Singh and Bala proposed a brain MRI image segmentation method based on Local Zernike Moment (LZM), a feature with good invariance [19].

2.1.3 Edge Characteristics

There is some variability in the marginal features of different organs in ultrasound dynamic images, for example, the uterus is generally an oval structure, the thyroid is generally butterfly or horseshoe shaped, and the spleen has a triangular vertebral shape. Currently, edge detection methods can be broadly classified into two categories: gradient-based lookup methods and zero crossing-based methods. The gradient-based lookup method requires finding the pixel points in the image that have the maximum and minimum values on the first-order derivative (gradient), and usually the pixel points in the direction with the largest gradient are used as boundary points. The first-order differential edge operator, also known as the gradient edge operator, is used for edge detection by exploiting the stepwise nature of the image at the edge, i.e., the property that the image gradient achieves a great value at the edge, specifically by selecting the widely used Sobel operator. The zero-crossing based method requires calculating the second order derivative of the image and detecting the boundary by whether the second order derivative is zero crossing or not, specifically by selecting the widely used Canny operator [20].

Qiao et al. proposed a robust edge extraction method based on edge-aware filtering and improved local binary pattern (EF-ALBP), which can handle CT images with more noise, blurred details and low contrast [21]. Elmi and Elmi proposed an edge detection method with a set hysteresis threshold that can be effectively applied for tracking and matching targets in colonoscopy detection [22]. Jie et al. proposed a salient structure based on the edge extraction operator XDoG for detecting gradients and energies of non-significant information in medical images of different modalities and fusing them into one medical image [23].

2.2 Feature Fusion

2.2.1 PCA Algorithm

PCA is a common data analysis method. PCA transforms the original data into a set of linearly independent representations of each dimension by linear transformation, which can be used to extract the main feature components of the data and is often used for dimensionality reduction operations of high-dimensional data. PCA works by sequentially finding a set of mutually orthogonal axes from the original space, and the choice of new axes is closely related to the data itself. The first new axis is chosen in the direction of the largest variance in the original data, the second new axis is chosen in the plane orthogonal to the first axis that makes the largest variance, and the third axis is in the plane orthogonal to the first, second axis that makes the largest variance. By analogy, n such axes can be obtained as the new axis system, so that only the dimensional features containing most of the variance are retained, while the dimensional features containing almost zero variance are ignored, and the dimensional reduction fusion of data features is realized.

2.2.2 TF-IDF Algorithm

The TF-IDF algorithm uses keywords to assess the importance in an article or a document. The importance of a keyword increases with the frequency of its occurrence and also decreases inversely with the frequency of its occurrence in the corpus. Term Frequency (TF) represents the frequency of keywords appearing in the document. Inverse Document Frequency (IDF) is the inverse of the keyword's occurrence inside all documents. For a document set or corpus, the fewer documents containing a word, the larger the value of IDF, and the stronger and more important the word's distinguishing power. The TF-IDF is calculated as: TF-IDF = number of occurrences of a word or phrase in a document/total number of words or phrases in the document $*$ log(number of documents/(number of documents containing the word or phrase) + 1).

Ding et al. designed an invariant subspace and subspace combination method to achieve robust multimodal medical image fusion [24]. Chen et al. proposed a pyramidal network model combining local edge features and global edge features to achieve automatic recognition of the central room of CT images [25]. Gudadhe et al. classified CT images of intracranial hemorrhage in stroke patients by combining Grey Level Co-occurrence Matrix (GLCM) features, Discrete Wavelet Features (DWT) and Discrete Cosine Features (DCT) [26]. Kuwil proposed the FE_mines (Feature Extraction Based on Region of Mines) method to extract effectively combined features in MRI images for effective brain tumour identification [27].

3 METHODS

During an ultrasound examination, with the movement of the probe, a variety of human tissues and organs are detected at different angles in the form of dynamic images displayed in the screen, and since the images have multiple features, different features contribute differently to the description of the images. As shown in Figure 1, several major examinations of ultrasound medicine were selected as the focus of this paper, with the categories *liver, gallbladder, spleen, pancreas* for PCA, *prostate, testes* for FF-IIF, and *uterus, ovaries* for TF-IDF.

This article analyzes the differences in texture, edge, and shape underlying features in human organ images collected by ultrasound medicine, and designs a model framework for ultrasound medical image classification based on multiple feature extraction and fusion, as shown in Figure 2. Firstly, various underlying features such as texture, shape, and edge of prominent targets in medical images are extracted. Then, an adaptive composite feature classification is generated using the FF-IIF multi feature fusion algorithm, aiming to adapt to the dynamic changes in the position and direction of the ultrasound probe and maintain a certain degree of fault tolerance and stability in the extracted features. Finally, a classification model is established to learn and analyze the underlying composite image feature components, forming an abstract high-level feature representation, achieving the goal of accurately, quickly and automatically analyzing various human tissues and organs in ultrasound medical images.

3.1 Initialization Data

The N tissues and organs appearing in the ultrasound dynamic image are classes, and the set of classes is $\{\mathrm{CLiver}, \mathrm{CGallbladder}, \mathrm{CSpleen}, \mathrm{CPancreas}\}$, and the specific object corresponding to the class is extracted accordingly for each class in

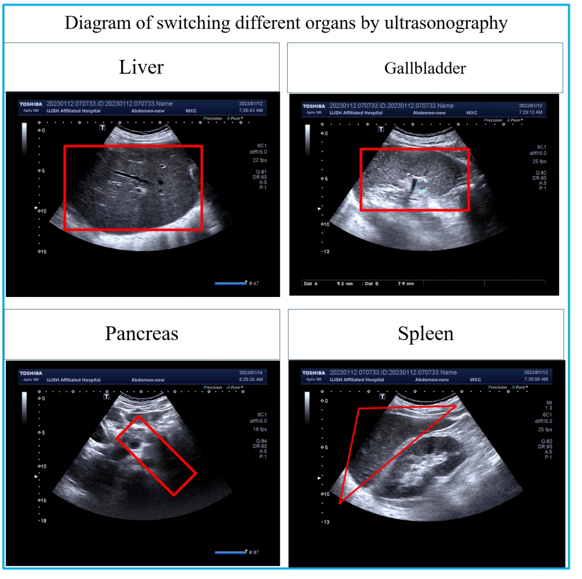

Figure 1. Schematic diagram of switching to different tissues and organs at the same ultrasound examination

the image set, as shown in Figure 1, CLiver class corresponds to the extraction of $\{\mathrm{Liver}_1, \mathrm{Liver}_2, \mathrm{Liver}_3, \ldots, \mathrm{Liver}_i\}$, CGallbladder class corresponds to the extraction of $\{\mathrm{Gallbladder}_1, \mathrm{Gallbladder}_2, \mathrm{Gallbladder}_3, \ldots, \mathrm{Gallbladder}_i\}$, CSpleen class corresponding to the extraction of $\{\mathrm{Spleen}_1, \mathrm{Spleen}_2, \mathrm{Spleen}_3, \ldots, \mathrm{Spleen}_i\}$, CPancreas class corresponding to the extraction of $\{\mathrm{Pancreas}_1, \mathrm{Pancreas}_2, \mathrm{Pancreas}_3, \ldots, \mathrm{Pancreas}_i\}$.

For each object separately, the values of the various characteristic components of its various angular forms are calculated as:

$$
\begin{gathered}
\mathrm{Gallbladder}_1 \left\{ \begin{matrix} (C_{111}, C_{211}, \ldots, C_{m11}), & (C_{112}, C_{212}, \ldots, C_{m12}) \\ (C_{113}, C_{213}, \ldots, C_{m13}), & (C_{11j}, C_{21j}, \ldots, C_{m1j}) \end{matrix} \right\} \\
\mathrm{Gallbladder}_2 \left\{ \begin{matrix} (C_{121}, C_{221}, \ldots, C_{m21}), & (C_{122}, C_{222}, \ldots, C_{m22}) \\ (C_{123}, C_{223}, \ldots, C_{m23}), & (C_{12j}, C_{22j}, \ldots, C_{m2j}) \end{matrix} \right\} \\
\mathrm{Gallbladder}_3 \left\{ \begin{matrix} (C_{131}, C_{231}, \ldots, C_{m31}), & (C_{132}, C_{232}, \ldots, C_{m32}) \\ (C_{133}, C_{233}, \ldots, C_{m33}), & (C_{13j}, C_{23j}, \ldots, C_{m3j}) \end{matrix} \right\} \\
\vdots \\
\mathrm{Gallbladder}_i \left\{ \begin{matrix} (C_{1i1}, C_{2i1}, \ldots, C_{mi1}), & (C_{1i2}, C_{2i2}, \ldots, C_{mi2}) \\ (C_{1i3}, C_{2i3}, \ldots, C_{mi3}), & (C_{1ij}, C_{2ij}, \ldots, C_{mij}) \end{matrix} \right\}.
\end{gathered} \tag{1}
$$

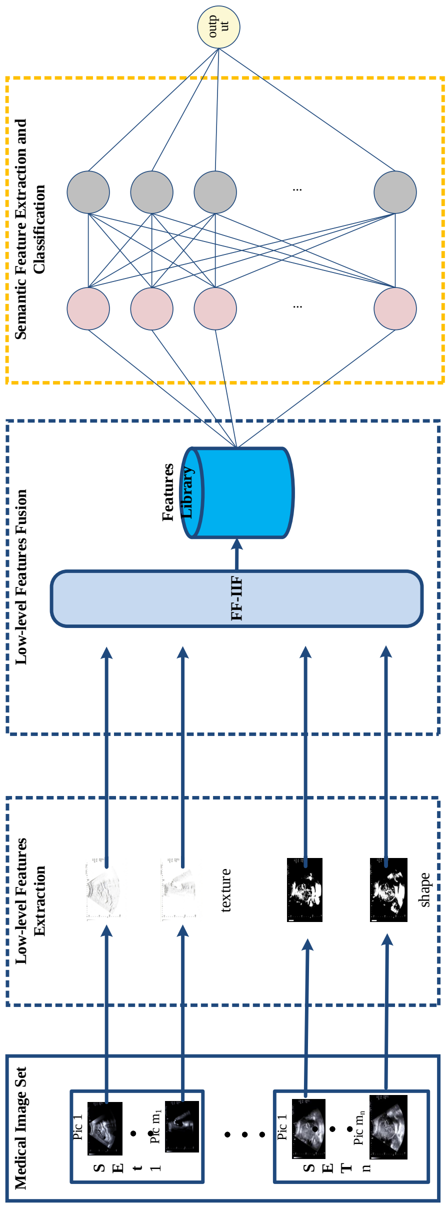

Figure 2. Framework diagrams of multiple features extraction and fusion method for ultrasound dynamic images

M is the initial number of adopted feature component dimensions, N is the number of all instance objects for the class, and Q is the number of various angular forms of instance objects, where $m \leq M$, $i \leq N$, and $j \leq Q$. The initial input data is obtained by unifying the various angles by means of the mean value method as follows:

$$C_{mi} = \frac{\sum_{j=1}^{Q} C_{mij}}{Q}. \tag{2}$$

Gallbladder$_1$ $(C_{11}, C_{21}, \ldots, C_{m1})$, Gallbladder$_2$ $(C_{12}, C_{22}, \ldots, C_{m2})$, Gallbladder$_3$ $(C_{13}, C_{23}, \ldots, C_{m3})$, $\ldots$, Gallbladder$_i$ $(C_{1i}, C_{2i}, \ldots, C_{mi})$.

3.2 Related Definitions

Definition 1 (Frequency)**.** C_m represents the feature component of the m^{th} object, and C_{mi} represents the i^{th} feature component value of the m^{th} object. The C_{mi} values of all tissue and organ objects are mapped to linear coordinates, and the mean $mid = \sum_{i=0}^{X} C_{mi}$ of all feature component values is calculated. The feature component value C_{mi} frequency is the number of feature components other than itself in the range of $C_{mi} - \frac{mid}{2} < x < C_{mi} + \frac{mid}{2}$.

Definition 2 (Feature Frequency)**.** The adjacent values of a feature component value in the same tissue-organ object; the more adjacent values, the more relevant the feature component value is to the feature representation of this tissue-organ object.

For example, the distribution of the C_{li} feature components of Gallbladder in various types of Gallbladder is shown in Figure 3. Then, for the range of C_{11} values of Gallbladder 1 can be matched to the C_{12} values of Gallbladder 2, so the value of FF of Gallbladder 1 is 1, and the value of FF of Gallbladder 2 is 2, the value of FF of Gallbladder 3 is 1, and the value of FF of Gallbladder 4 is 0.

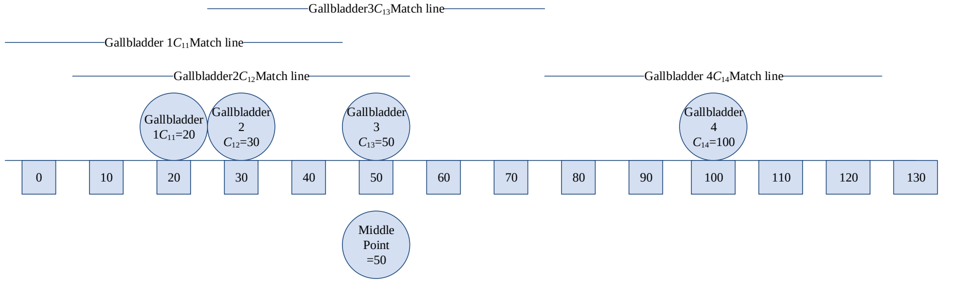

Figure 3. Schematic diagram of similar frequency calculation

Definition 3 (Inverse Image Frequency)**.** The values of a feature component value adjacent to each other in different tissue-organ object matches; the more values adjacent to each other, the less distinguishing ability of that feature component value.

For example, if an experimental data includes 100 sample data, and the feature component value C_{m1} appears 10 times in different tissue-organ object matches, and another feature component value C_{m2} appears 1 time in different tissue-organ object matches, then C_{m2} has better discrimination than C_{m1}.

The FF-IIF value for each feature component value is calculated using the above concept, using Equation (3):

$$\text{FF-IIF}(C_{mi}) = ff_j\left(C_{mi}\right) \times \log\left[\frac{N}{iif\left(C_{mi}\right)}\right], \tag{3}$$

where $\iint_j\left(C_{mi}\right)$ denotes the frequency of occurrence of the characteristic component value C_{mi} in the same tissue-organ object; N denotes the total number of all tissue-organ objects in the set of tissue-organ objects; $iif(C_{mi})$ denotes the frequency of the current feature component values occurring in different tissue organ object collections. By analyzing each feature component value in the tissue organ object collection as described above, the FF-IIF value of each feature component value for each tissue organ object is obtained, and then the value is used to build a vector model for each tissue organ object separately as the classification criteria of the features and the correlation test for each dimension.

3.3 Calculation Method

Since the situation discussed in this paper requires high compatibility of the characteristic components of tissue and organ objects is not very numerically sensitive and different ultrasound equipment may have different resolutions, it does not require too complicated calculation and refinement problems. From the initial feature component value C'_{mi}, representing the i^{th} initial feature component value of the m^{th} object in the ultrasound examination, the feature component value C_{mi}, representing the i^{th} feature component value of the m^{th} object, is calculated by taking the absolute value and logarithm of the feature component according to Equation (4).

$$C_{mi} = \log|C'_{mi}|. \tag{4}$$

After the pre-processing of the feature component values is completed the FF-IIF value of each feature component value of each tissue organ object in the whole tissue organ object collection needs to be calculated, and the FF-IIF value of each feature component value of the tissue organ object is expressed as a vector, and the similarity of the tissue organ object is calculated. This vector is high-dimensional and extremely sparse. According to information theory, the IIF value is actually the cross entropy of the probability distribution of feature component values under a particular condition, while FF is used to increase the weight of the feature component values to better characterize the data of the feature component values in the tissue organ object. Therefore, a number of important feature component values can be selected from each tissue organ object as a way to characterize the tissue organ object to ensure that the dimensionality of the tissue organ object feature vector representation can be minimized without affecting the tissue organ object feature extraction. This is done by ranking the FF-IIF values of the feature component values in each tissue organ object. The feature component value from which the FF-IIF value is greater than the elimination threshold P (percentage) is selected as the key feature component value. This key component value is used as the feature representation of the tissue object, and the efficiency of the algorithm is greatly improved due to the dimensionality reduction operation.

After obtaining the key feature component values for each tissue and organ object, it is then necessary to consider how to determine the calculation of the weight of the feature component values for a particular category of ultrasound examination. Since the feature component values represent the most important features in a tissue-organ object, the feature component value weights of ultrasonography can be derived statistically from the feature component value weights of tissue-organ objects, and the feature component value weights of a certain class of ultrasonography are converted into a statistical work on the feature component value weights of tissue-organ objects. In addition, since each tissue and organ object has different types of features, the dimensions of the feature component weights characterizing the ultrasound examination are not the same, and these effects must be eliminated so that the feature component weights of a certain type of ultrasound examination satisfy the feature types of each tissue and organ object.

Let w_i, w_j be the distribution of the feature component value weights of two different tissue organ objects, $w_i = \{w_{1i}, w_{2i}, \ldots, w_{mi}\}$, $w_j = \{w_{1j}, w_{2j}, \ldots, w_{mj}\}$, where M is the number of all feature component values, $m \leq M$.

If there are more feature component values that are more similar to each other in two tissue organ objects and the higher the proportion of FF-IIF values accounted for by the feature component values in the respective tissue organ objects – it means that these feature component values are more reflective of their importance in the tissue organ objects, so the weights are calculated based on the proportion of FF-IIF values of key feature component values that satisfy the similarity threshold condition in the key feature component values in the sum of FF-IIF values of the whole tissue organ objects. The specific calculation formula is given by Equation (5).

$$w_{i,j} = 1 + \mathrm{avg}(i,j) \times \left[\sqrt{\mathrm{avg}(i,j)} - \mathrm{avg}(i,j)\right], \tag{5}$$

$$\mathrm{avg}\,(i,j) = \frac{1}{2}\left[\frac{\sum_{k\in\Lambda_i}\text{FF-IIF}\,(C_{ik})}{\sum_{k=1}^{M}\text{FF-IIF}\,(C_{ik})} + \frac{\sum_{l\in\Lambda_j}\text{FF-IIF}\,(C_{jl})}{\sum_{l=1}^{M}\text{FF-IIF}\,(C_{jk})}\right], \tag{6}$$

where FF-IIF(C_{ik}) denotes the FF-IF value of the key feature component value C_{ik}, $\wedge_i$ is the set of key feature component value weights w_{jl} whose similarity exceeds the similarity threshold μ set by the user.

$$\wedge_i = \left\{ k : 1 \leq k \leq m, \max_{1 \leq l \leq n} \{\arg(i,j)\} \geq \mu \right\}. \tag{7}$$

This feature component vector weight value is calculated as follows:

$$wf = \frac{\sum_{i=1}^{M} \sum_{j=1}^{N} w_{i,j}}{M^{*}N}. \tag{8}$$

The values of all feature components $\{wf_1, wf_2, \ldots, wf\}$ are calculated for this image selection in turn.

The machine learning model receives feature components $\{wf_1, wf_2, \ldots, wf\}$ as its input and calculates the predicted classification category as output of different tissues and organs in the ultrasound examination.

4 EXPERIMENTAL DETAILS

To verify the effectiveness of the FF-IIF algorithm proposed in this paper for the underlying multi-feature fusion of ultrasound dynamic images, ultrasound dynamic images of various tissues and organs in PCA, TF-IDF, and FF-IIF were selected for experiments and discussions, and then the effects of different feature fusions in the method on the overall framework performance were analyzed.

4.1 Experimental Environment

4.1.1 Experimental Data

The ultrasound dynamic image data used in this paper were provided by the hospital, with a total of 500 dynamic images, and the annotated data were manually annotated by professional medical field experts organized by the hospital. According to the guidelines and norms of ultrasound medicine, experts in the medical field defined a total of 10 classifications as: "liver", "bile", "pancreas", "spleen", "kidney", "bladder", "seminal vesicle gland", "prostate", "ovaries", "uterus".

4.1.2 Experimental Environment

The hardware environment and software used in this paper are hardware environment: VM-Ware virtual machine cluster 10, memory 32 GB, 8-core CPU; operating system: Windows Server 2012; deep learning tools: tensorflow, Keras; algorithm programming and interface display: Python, JSP, Visual C# 2010.

4.2 Comparison of Underlying Feature Fusion Performance

To verify the effectiveness of the FF-IIF algorithm proposed in this paper for the fusion of multiple features in the underlying layers of ultrasound dynamic images, a total of 36 components in 8 categories of underlying features were selected for testing, as shown in Table 1.

4.2.1 Visualization of Ultrasound Dynamic Image Features

Figure 4 gives the results of visualizing the characteristics of each tissue and organ by ultrasonography, where Figure 4 a) is the image frame in the ultrasound dynamic image, and the labeled rectangular box is the tissue and organ region. Figures 4 b) and 4 c) are the visualized heat maps of texture and shape regions, respectively, and Figure 4 d) is the visualized heat map after texture and shape fusion. It can be seen from the figure that the shape feature regions of the liver and kidney are not obvious, while the texture features are more obvious; the texture feature regions of the uterus and gallbladder are not obvious, while the shape regions are obvious. Compared with the texture and regional features alone, the fused features are closer to the location of the tissue-organ regions.

4.2.2 Elimination Threshold P-Value

The choice of the elimination threshold P-value directly affects the number of selected features, and the effectiveness of the combined feature component selection. If the P-value is chosen too large, some contributing feature components will be sacrificed, and if the P-value is chosen too small, some less obvious feature components will be left behind, so the P-value is chosen too large or too small to be detrimental to the selection of feature components. In this paper, the size of P-value is determined by comparing the effect of experimental tests.

From Table 2, it can be seen that the recognition performance of the selected combined feature components is better when the value of P is 0.5 for PCA, and the final selected combined feature components are 15, the recognition performance of the selected combined feature components is better when the value of P is 0.6 for TF-IDF, and the final selected combined feature components are 9, and the recognition performance of the selected combined feature components is better when the value of P is 0.5 for FF-IIF, and the final selected combined feature components are 14, which also shows that the combined feature components have better recognition performance for FF-IIF.

4.2.3 Similarity Threshold

The size of the similarity threshold μ directly affects the calculation results of the feature component weights and thus the final recognition rate calculation. In this paper, the similarity threshold μ in each medical examination item is selected by means of experiments. As shown by the experimental results in Figure 5, the highest recognition rate was obtained when the value of μ was 0.8 for PCA, when the value of μ was 0.7 for FF-IIF, and when the value of μ was 0.6 for TF-IDF. FF-IIF achieves the best recognition rate.

Eigenvalue Name	Variable Name	Type	Portion Name
Contrast ratio (grayscale co-occurrence)	GContrast	Grayscale co-occurrence matrix texture features	C1
Autocorrelation coefficient	GAutocorrelation	Grayscale symbiotic matrix texture features	C2
Degree of difference	GDissimilarity	Grayscale symbiotic matrix texture features	C3
Energy	GEnergy	Grayscale symbiotic matrix texture features	C4
Entropy	GEntropy	Grayscale symbiotic matrix texture features	C5
Homogeneity	GHomogeneity	Grayscale symbiotic matrix texture features	C6
Variance	GVariance	Grayscale symbiotic matrix texture features	C7
Covariance and	GSumvariance	Grayscale symbiotic matrix texture features	C8
Correlation coefficient	GCorrelation	Grayscale symbiotic matrix texture features	C9
Contrast (Tamura)	TContrast	Tamura texture features	C10
Directionality	TCoarseness	Tamura texture features	C11
Roughness	TDir	Tamura texture features	C12
Hu invariant moment1	H1	Hu Invariant Moment Feature	C13
Hu constant moment2	H2	Hu Invariant Moment Feature	C14
Hu constant moment3	H3	Hu invariant moment feature	C15
Hu constant moment4	H4	Hu invariant moment feature	C16
Hu constant moment5	H5	Hu Invariant Moment Feature	C17
Hu constant moment6	H6	Hu Constant Moment Characteristics	C18
Hu constant moment7	H7	Hu invariant moment characteristics	C19
Radius-invariant moment1	V1	Polar Radius Invariant Moment	C20
Radius-invariant moment 2	V2	Polar Radius Invariant Moment Characteristics	C21
Constant moment 3	V3	Polar Radius Invariant Moment Characteristics	C22
Constant moment 4	V4	Polar Radius Invariant Moment Characteristics	C23
Polar radius invariant moment5	V5	Polar radius invariant moment characteristic	C24
Complex constant moment1	T1	Complex constant moment characteristics	C25
Complex constant moment 2	T2	Complex invariant moments	C26
Complex constant moment 3	T3	Complex constant moment characteristics	C27
Complex constant moment 4	T4	Complex invariant moment characteristics	C28
Complex constant moment 5	T5	Complex invariant moment characteristics	C29
Complex constant moment 6	T6	Complex invariant moment characteristics	C30
Complex invariant moment7	T7	Complex invariant moment characteristics	C31
Orthogonal invariant moment	L	Orthogonal invariant moment feature	C32
Gradient	SG	Sobel operator edge feature	C33
Direction	SD	Sobel operator edge feature	C34
Edge strength	CA	Canny operator edge feature	C35
Normal vector	CN	Canny operator edge feature	C36

Table 1. Representation of all selected eigenvalues

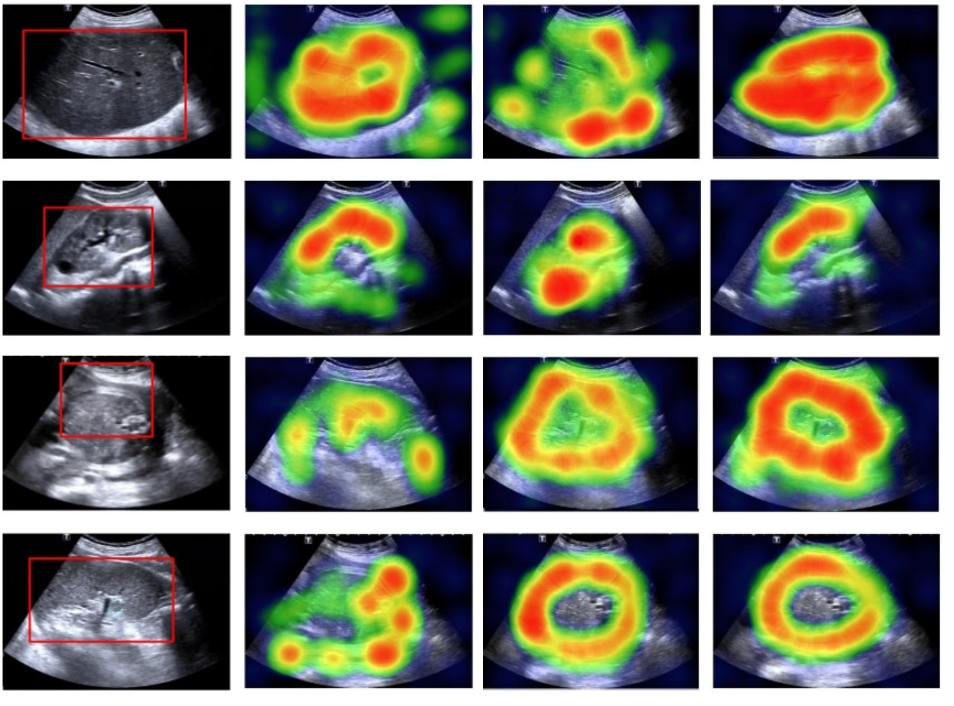

Figure 4. Example of heat map visualization of the underlying features of various organs in image frames of ultrasound dynamic images

4.2.4 Feature Component Weights

The feature component weight surfaces obtained after the algorithmic process of PCA, TF-IDF and FF-IIF algorithm are shown in Figure 6. By observation, it can be seen that the feature component weight fold surfaces of different inspection items have very significant differences, thus reflecting that the feature components of different inspection items contribute differently to the recognition of tissue organ objects in that item.

After the reselection of feature components in the PCA, TF-IDF and FF-IIF algorithm, the results are obtained as shown in Figure 7, which shows that the feature component weight of FF-IIF algorithm folded surface is relatively smooth, indicating that the adaptive elimination measures for the feature components can reduce the personality differences of different feature components and select representative feature components for combination, which has achieved the best classification effect.

***P*-Value**	**Number of Characteristic Subscales of PCA**	**PCA Recognition Rate**	**Number of TF-IDF Characteristic Subscales**	**TF-IDF Recognition Rate**	**Number of FF-IIF Characteristic Subscales**	**FF-IIF Recognition Rate**
0.9	3	0.34	3	0.45	4	0.50
0.8	6	0.48	5	0.51	5	0.53
0.7	8	0.62	7	0.43	7	0.65
0.6	10	0.70	9	0.81	11	0.76
0.5	15	0.90	13	0.71	14	0.79
0.4	16	0.79	15	0.59	17	0.68
0.3	19	0.68	19	0.45	21	0.60
0.2	21	0.58	28	0.39	29	0.54
0.1	34	0.32	33	0.37	34	0.43

Table 2. Comparison table of the number of selected feature components and recognition rate under different P-values

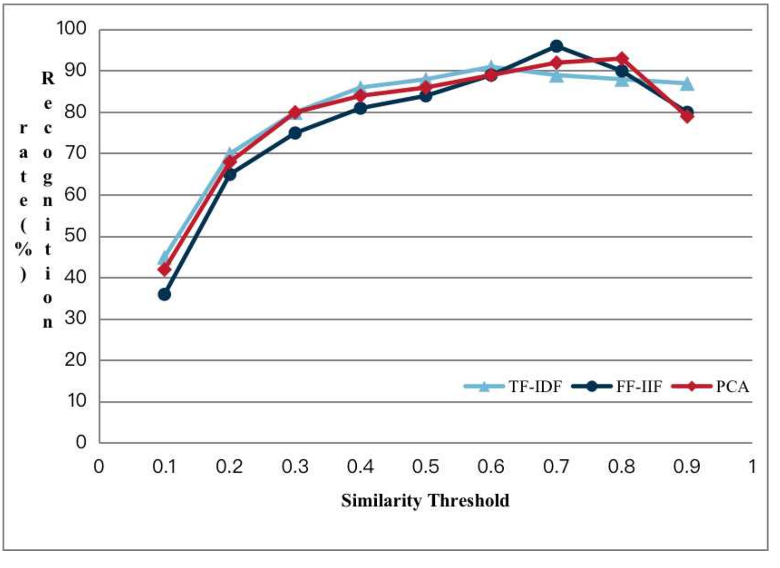

Figure 5. Schematic diagram of recognition rate influenced by similarity threshold

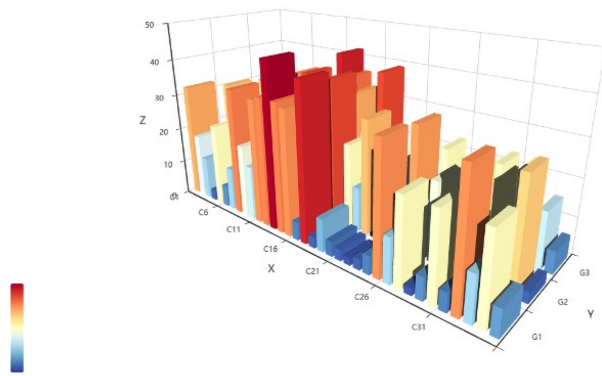

a) PCA

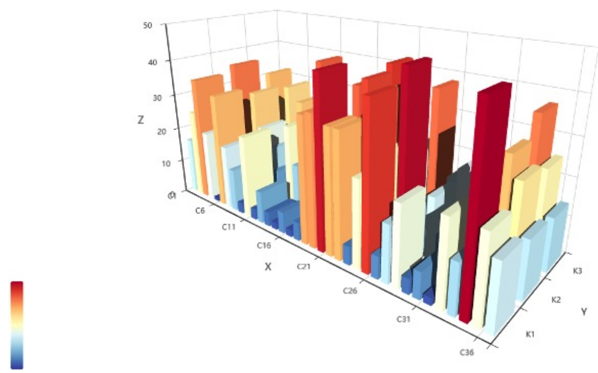

b) TF-IDF

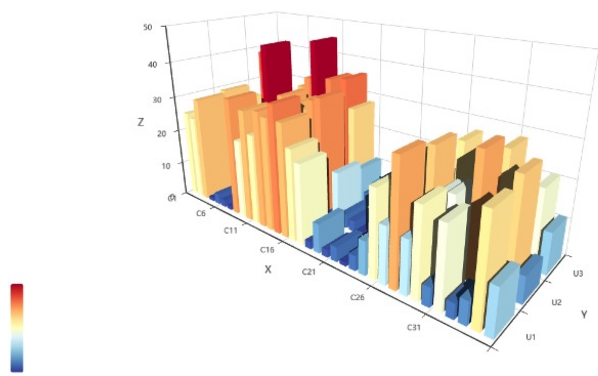

c) FF-IIF

Figure 6. Surface display of feature component weights of different inspection items

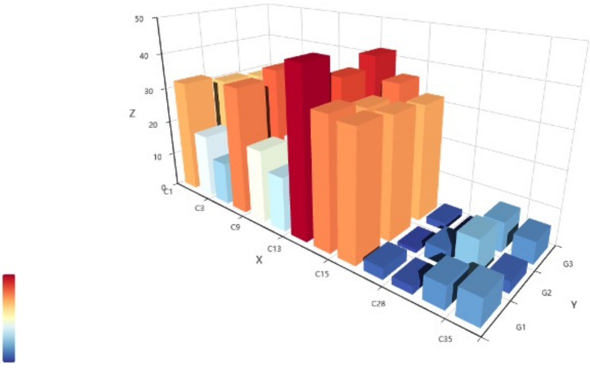

a) PCA

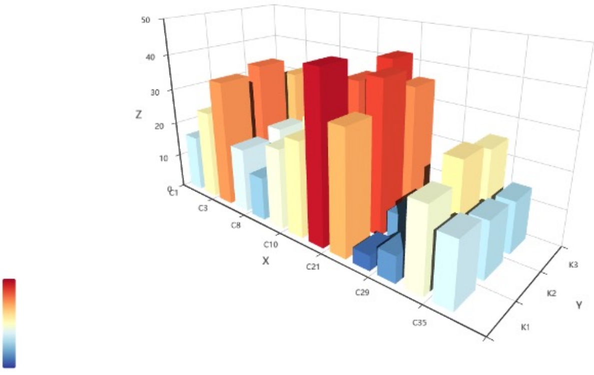

b) TF-IDF

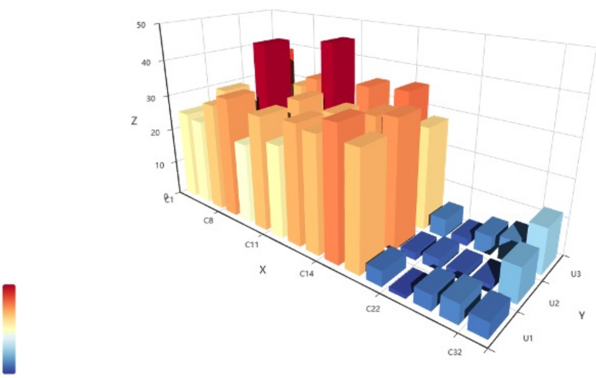

c) FF-IIF

Figure 7. Adaptive feature component weight surface display for different examination items

4.2.5 Feature Component Time Efficiency

To verify the running time efficiency of the PCA, TF-IDF, FF-IIF multi-feature fusion algorithm proposed in this paper, the extraction time of each feature was counted, as shown in Table 3.

Table 3 shows the statistics of the time required for the methods used for feature extraction, and it can be seen that the computation time for all types of feature components of the grayscale co-occurrence matrix is less than 1.00E+02 ms, and the average computation time spent is less, and the energy of the grayscale co-occurrence matrix has the least computation time by log. While the Tamura texture features have more multiplication operations, so the computation time of the associated feature variables is more than that of the grayscale coeval matrix. Hu invariant moment processing requires the calculation of seven moments, while the polar radius invariant moment only requires the calculation of five, so the polar radius invariant moment running time is relatively minimal. The average computation time of the polar radius invariant moments is close to the average computation time of each type of feature component of the grayscale co-occurrence matrix. Both complex invariant moments and orthogonal invariant moments are derived from the Hu invariant moment calculation criterion and therefore they take more time than the Hu invariant moment calculation. The Canny operator edge feature computation involves convolution operations, which are larger than the average computation time of the Sobel operator edge features. The computation time for all types of feature components is less than 4.00E+02 ms, which basically satisfies the computational requirements of the model. FF-IIF algorithm has the least total computation time.

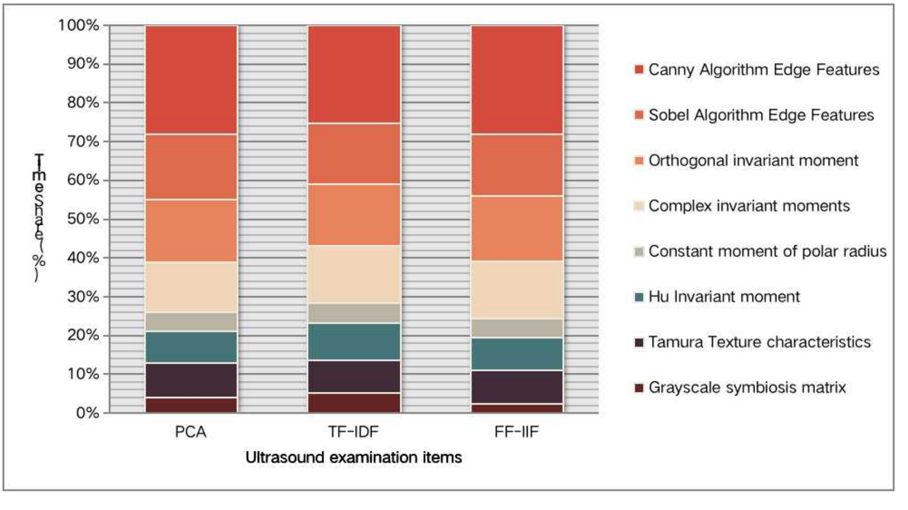

Figure 8. Average time share of each type of feature in ultrasound examination items

Characteristic Components	**Portion Name**	**PCA**	**TF-IDF**	**FF-IIF**
Contrast ratio (grayscale co-occurrence)	C1	2.40E+01	1.70E+01	1.50E+01
Autocorrelation coefficient	C2	1.30E+01	9.00E+00	8.00E+00
Degree of difference	C3	8.00E+00	7.00E+00	6.00E+00
Energy	C4	7.00E+00	4.00E+00	5.00E+00
Entropy	C5	3.10E+01	2.30E+01	2.10E+01
Homogeneity	C6	1.60E+01	8.00E+00	7.00E+00
Variance	C7	3.10E+01	1.90E+01	1.80E+01
Covariance and	C8	9.00E+00	7.00E+00	7.00E+00
Correlation coefficient	C9	4.60E+01	2.90E+01	2.60E+01
Contrast (Tamura)	C10	7.30E+01	5.90E+01	5.40E+01
Directionality	C11	1.40E+01	7.00E+00	5.00E+00
Roughness	C12	4.80E+01	3.40E+01	3.10E+01
Hu invariant moment 1	C13	4.50E+01	1.60E+01	1.40E+01
Hu constant moment 2	C14	8.50E+01	6.50E+01	5.70E+01
Hu constant moment 3	C15	9.20E+01	7.90E+01	7.40E+01
Hu constant moment 4	C16	9.30E+01	8.50E+01	8.00E+01
Hu constant moment 5	C17	1.10E+02	9.90E+01	9.70E+01
Hu constant moment 6	C18	9.80E+01	9.20E+01	8.60E+01
Hu constant moment 7	C19	1.41E+02	1.21E+02	1.10E+02
Radius-invariant moment 1	C20	2.50E+01	1.40E+01	1.20E+01
Radius-invariant moment 2	C21	2.60E+01	1.50E+01	1.20E+01
Constant moment 3	C22	3.00E+01	1.80E+01	1.70E+01
Constant moment 4	C23	3.20E+01	1.90E+01	1.80E+01
Polar radius invariant moment5	C24	3.90E+01	2.50E+01	2.30E+01
Complex constant moment 1	C25	1.56E+02	1.03E+02	9.20E+01
Complex constant moment 2	C26	2.23E+02	1.45E+02	1.23E+02
Complex constant moment 3	C27	3.21E+02	2.03E+02	1.93E+02
Complex constant moment 4	C28	2.56E+02	1.65E+02	1.38E+02
Complex constant moment 5	C29	2.86E+02	1.72E+02	1.56E+02
Complex constant moment 6	C30	2.62E+02	1.71E+02	1.43E+02
Complex invariant moment7	C31	2.61E+02	1.69E+02	1.42E+02
Orthogonal invariant moment	C32	3.21E+02	2.19E+02	2.15E+02
Gradient	C33	1.21E+02	1.06E+02	9.80E+01
Direction	C34	1.09E+02	9.90E+01	9.20E+01
Edge strength	C35	3.14E+02	2.95E+02	2.89E+02
Normal vector	C36	2.94E+02	2.76E+02	2.65E+02
Total computation time		4.06E+03	2.99E+03	2.75E+03

Table 3. Statistics of the time required for feature extraction (average running time [ms])

Figure 8 shows the average share of time spent on each ultrasound examination item for each type of feature in the experiment. On the one hand, it can be seen that the two types of edge features, orthogonal invariant moments and complex invariant moments, occupy a higher share of time due to their higher computational complexity, but do not exceed 30% of the total time. The other underlying features have a more equal share of computation time. On the other hand, it is also evident that the computational time shares of various types of features remain basically the same in the three different items of ultrasonography, indicating that the computational workload of FF-IIF algorithm of graph features is relatively stable without abnormal time-consuming situations.

As shown in Figure 9, the computation time of texture features and Hu-invariant moments is slightly shortened because the fused features are computed in multi-threaded parallel simultaneous computation mode, the orthogonal invariant moments and complex invariant moments are computed on the basis of Hu-invariant moments, which also shortens the computation time, and the leading formula of edge features is consistent, which reduces part of the computation time. Combined, the computation method using fused feature components can be reduced to about 60% of the time share of independently computed feature components, which reduces the computation time. The FF-IIF multi-feature fusion algorithm increases the computation time of weights based on the independent feature computation, so its computation time is longer than the independent feature computation, but the adaptive combination feature component streamlines some of the feature components by the preliminary computation, especially some higher-order feature components that consume more time, so its computation time is moderate and fully adapted to the real-time inspection of ultrasound medicine.

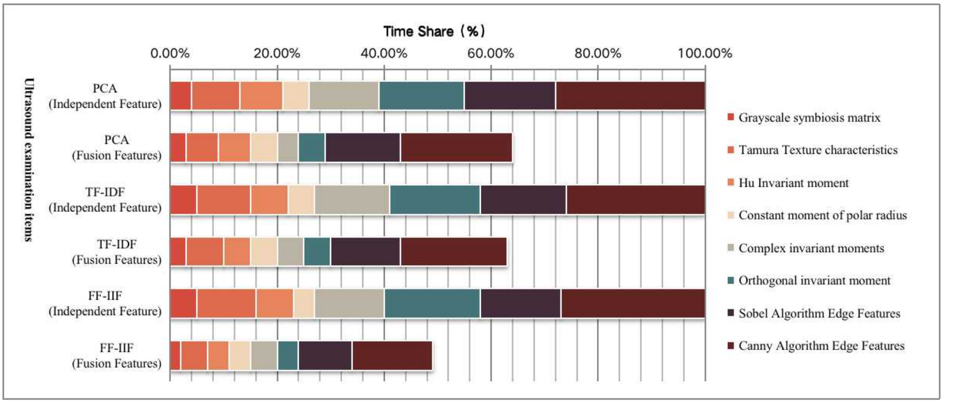

Figure 9. Time share of independent and post-fusion feature components in ultrasound examination items

5 CONCLUSION

In this paper, based on the analysis of the current status of research on the selection of underlying features for ultrasound examination organ characterization, the characteristics of various types of underlying features are introduced and the calculation formulas for various types of representative features are given. In order to solve the redundancy and selection problems of various components of multiple features in the underlying medical dynamic image, an adaptive combination multi-feature fusion method is proposed, and the FF-IIF method is defined to calculate the weight values of the feature components of tissues and organs in medical examination items. Firstly, all the feature components are combined together after initialization, then the FF-IIF value of each object is calculated by the FF-IIF method by sorting the FF-IIF values of each object, filtering out the redundant or even useless feature components after thresholding, and finally combining the feature components and the weight values of the feature components to generate the initial data before classification. Two thresholds FF-IIF in elimination threshold P-value and similarity threshold μ were calculated in the experiments, and the FF-IIF algorithm was performed for inspection items.

Future work will focus on two main areas:

1. It is noteworthy that more and more image processing fields are beginning to employ reinforcement learning to discover more feature components that can describe and classify images. The future task is to explore more underlying feature components suitable for ultrasound dynamic images and provide them to the classification model to achieve better classification results.

2. The multi-feature fusion algorithm we currently use works better for fusing the underlying features describing tissue and organ lesions in existing ultrasound dynamic images. However, with the appearance of more underlying features, it may have some impact on the computational performance and effect of the algorithm proposed in this paper, so the existing algorithm needs to be further optimized to achieve a better fusion effect.

Funding

This research was funded by the National Natural Science Foundation of China, Grant No. 61976107; Major Project of Philosophy and Social Science Research in Higher Education Institutions in Jiangsu Province, Grant No. 2023SJZD026; Zhenjiang policy guidance plan, grant No. RK2022004; Zhenjiang policy guidance plan, Grant No. RK2023011; Research Project on Refined Management and Evaluation of Public Hospitals in National Health Commission, Grant No. NIHA23JXH031.

REFERENCES

[1] Santarelli, M. F.—Giovannetti, G.—Hartwig, V.—Celi, S.—Positano, V.—Landini, L.: The Core of Medical Imaging: State of the Art and Perspectives on the Detectors. Electronics, Vol. 10, 2021, No. 14, Art. No. 1642, doi: 10.3390/electronics10141642.

[2] Suetens, P.: Fundamentals of Medical Imaging. 2nd Edition. Cambridge University Press, 2009, doi: 10.1017/CBO9780511596803.

[3] Liu, S.—Chai, Q.—Zheng, W.: Automatic Tracking of Muscle Fiber Direction in Ultrasound Images Based on Improved Kalman Filter. Electronics, Vol. 11, 2022, No. 3, Art. No. 466, doi: 10.3390/electronics11030466.

[4] Graziani, M.—Eggel, I.—Deligand, F.—Bobák, M.—Andrearczyk, V.—Mueller, H.: Breast Histopathology with High-Performance Computing and Deep Learning. Computing and Informatics, Vol. 39, 2020, No. 4, pp. 780–807, doi: 10.31577/cai_2020_4_780.

[5] Maqsood, S.—Damaševičius, R.—Shah, F. M.—Maskeliunas, R.: Detection of Macula and Recognition of Aged-Related Macular Degeneration in Retinal Fundus Images. Computing and Informatics, Vol. 40, 2021, No. 5, pp. 957–987, doi: 10.31577/cai_2021_5_957.

[6] Lowe, D. G.: Distinctive Image Features from Scale-Invariant Keypoints. International Journal of Computer Vision, Vol. 60, 2004, pp. 91–110, doi: 10.1023/B:VISI.0000029664.99615.94.

[7] Trinh, D. L.—Kim, S. H.—Yang, H. J.—Lee, G. S.: The Efficacy of Shape Radiomics and Deep Features for Glioblastoma Survival Prediction by Deep Learning. Electronics, Vol. 11, 2022, No. 7, Art. No. 1038, doi: 10.3390/electronics11071038.

[8] Adjailia, F.—Ramdani, M.—Rasamoelina, A. D.—Sincak, P.: Integration of 2D Textural and 3D Geometric Features for Robust Facial Expression Recognition. Computing and Informatics, Vol. 40, 2021, No. 5, pp. 988–1007, doi: 10.31577/cai_2021_5_988.

[9] He, B.—Liu, J.—Lin, G.—Peng, C.—Xi, W.: Quaternion Fractional-Order Weighted Generalized Laguerre-Fourier Moments and Moment Invariants for Color Image Analysis. Signal Processing: Image Communication, Vol. 114, 2023, Art. No. 116941, doi: 10.1016/j.image.2023.116941.

[10] Liu, R.—Nan, H.—Zou, Y.—Xie, T.—Ye, Z.: LSW-Net: A Learning Scattering Wavelet Network for Brain Tumor and Retinal Image Segmentation. Electronics, Vol. 11, 2022, No. 16, Art. No. 2616, doi: 10.3390/electronics11162616.

[11] Calhoun, V. D.—Adali, T.: Feature-Based Fusion of Medical Imaging Data. IEEE Transactions on Information Technology in Biomedicine, Vol. 13, 2009, No. 5, pp. 711–720, doi: 10.1109/TITB.2008.923773.

[12] Tran, D. C.—Wu, Z.: A New Approach of Dynamic Clustering Based on Particle Swarm Optimization and Application in Image Segmentation. Computing and Informatics, Vol. 36, 2017, No. 3, pp. 637–663, doi: 10.4149/cai_2017_3_637.

[13] Zhai, Z.—Fan, C.—Ming, Y.: Learned Spatio-Temporal Texture Descriptors for RGB-D Human Action Recognition. Computing and Informatics, Vol. 37, 2018, No. 6, pp. 1339–1362, doi: 10.4149/cai_2018_6_1339.

[14] Rogers, W.—Keek, S. A.—Beuque, M.—Lavrova, E.—Primakov, S.—Wu, G.—Yan, C.—Sanduleanu, S.—Gietema, H. A.—Casale, R.—Occhipinti, M.—Woodruff, H. C.—Jochems, A.—Lambin, P.: Towards Texture Accurate Slice Interpolation of Medical Images Using PixelMiner. Computers in Biology and Medicine, Vol. 161, 2023, Art. No. 106701, doi: 10.1016/j.compbiomed.2023.106701.

[15] Feng, Y.—Wu, J.—Hu, X.—Zhang, W.—Wang, G.—Zhou, X.—Zhang, X.: Medical Image Fusion Using Bilateral Texture Filtering. Biomedical Signal Processing and Control, Vol. 85, 2023, Art. No. 105004, doi: 10.1016/j.bspc.2023.105004.

[16] Santos, J. D.—de M. S. Veras, R.—Silva, R. R. V.—Aldeman, N. L. S.—Araújo, F. H. D.—Duarte, A. A.—Tavares, J. M. R. S.: A Hybrid of Deep and Textural Features to Differentiate Glomerulosclerosis and Minimal Change Disease from Glomerulus Biopsy Images. Biomedical Signal Processing and Control, Vol. 70, 2021, Art. No. 103020, doi: 10.1016/j.bspc.2021.103020.

[17] Kawashima, Y.—Miyakoshi, M.—Kawabata, Y.—Indo, H.: Efficacy of Texture Analysis of Ultrasonographic Images in the Differentiation of Metastatic and Non-Metastatic Cervical Lymph Nodes in Patients with Squamous Cell Carcinoma of the Tongue. Oral Surgery, Oral Medicine, Oral Pathology and Oral Radiology, Vol. 136, 2023, No. 2, pp. 247–254, doi: 10.1016/j.oooo.2023.04.012.

[18] Li, X.—Yin, Y.—Feng, R.—Yu, J.—Cao, D.—Wu, X.—Wang, W.: Double Total Variation (DTV) Regularization and Improved Adaptive Moment Estimation (IADAM) Optimization Method for Fast MR Image Reconstruction. Computer Methods and Programs in Biomedicine, Vol. 233, 2023, Art. No. 107463, doi: 10.1016/j.cmpb.2023.107463.

[19] Singh, C.—Bala, A.: An Unsupervised Orthogonal Rotation Invariant Moment Based Fuzzy C-Means Approach for the Segmentation of Brain Magnetic Resonance Images. Expert Systems with Applications, Vol. 164, 2021, Art. No. 113989, doi: 10.1016/j.eswa.2020.113989.

[20] Wójtowicz, T.—Bułka, D.: Ellipse Detection in Forensic Blood Stain Images Analysis. Computing and Informatics, Vol. 37, 2018, No. 1, pp. 213–228, doi: 10.4149/cai_2018_1_213.

[21] Qiao, S.—Yu, Q.—Zhao, Z.—Song, L.—Tao, H.—Zhang, T.—Zhao, C.: Edge Extraction Method for Medical Images Based on Improved Local Binary Pattern Combined with Edge-Aware Filtering. Biomedical Signal Processing and Control, Vol. 74, 2022, Art. No. 103490, doi: 10.1016/j.bspc.2022.103490.

[22] Elmi, S.—Elmi, Z.: A Robust Edge Detection Technique Based on Matching Pursuit Algorithm for Natural and Medical Images. Biomedical Engineering Advances, Vol. 4, 2022, Art. No. 100052, doi: 10.1016/j.bea.2022.100052.

[23] Jie, Y.—Li, X.—Zhou, F.—Tan, H.: Medical Image Fusion Based on Extended Difference-of-Gaussians and Edge-Preserving. Expert Systems with Applications, Vol. 227, 2023, Art. No. 120301, doi: 10.1016/j.eswa.2023.120301.

[24] Ding, Z.—Li, H.—Guo, Y.—Zhou, D.—Liu, Y.—Xie, S.: M4FNet: Multimodal Medical Image Fusion Network via Multi-Receptive-Field and Multi-Scale Feature Integration. Computers in Biology and Medicine, Vol. 159, 2023, Art. No. 106923, doi: 10.1016/j.compbiomed.2023.106923.

[25] Chen, S.—Qiu, C.—Yang, W.—Zhang, Z.: Combining Edge Guidance and Feature Pyramid for Medical Image Segmentation. Biomedical Signal Processing and Control, Vol. 78, 2022, Art. No. 103960, doi: 10.1016/j.bspc.2022.103960.

[26] Gudadhe, S.—Thakare, A.—Anter, A. M.: A Novel Machine Learning-Based Feature Extraction Method for Classifying Intracranial Hemorrhage Computed Tomography Images. Healthcare Analytics, Vol. 3, 2023, Art. No. 100196, doi: 10.1016/j.health.2023.100196.

[27] Kuwil, F. H.: A New Feature Extraction Approach of Medical Image Based on Data Distribution Skew. Neuroscience Informatics, Vol. 2, 2022, No. 3, Art. No. 100097, doi: 10.1016/j.neuri.2022.100097.

Xiaojun Chen is Professor of informatics at the Affiliated Hospital of Jiangsu University, in Zhenjiang, the Jiangsu province, China. Meanwhile, he is a doctoral candidate (studying) of the School of Computer Science and Communication Engineering of Jiangsu University. He received his Master's degree in computer application and Bachelor's degree in software design both from the Jiangsu University in 2007 and 2004, respectively. His main research interests focus on pattern recognition and image processing.

Jia Ke is Assistant Professor of informatics at the School of Business Administration of Jiangsu University, in Zhenjiang, the Jiangsu province, China. She received her Doctor's degree, Master's degree and Bachelor's degree from the School of Computer Science of Jiangsu University in 2013, 2007 and 2004, respectively. Her main research interests focus on pattern recognition and image processing.

Yaning Zhang is an undergraduate of the Jiangsu University, in Zhenjiang, the Jiangsu province, China, and his main research interest is medical image recognition and classification.

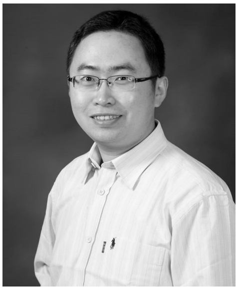

Lu Liu is Professor of informatics at the University of Leicester, U.K. He received his Ph.D. degree from the University of Surrey (U.K.) and his M.Sc. in data communication systems from the Brunel University (U.K.). He is currently serving as Associate Editor for Peer-to-Peer Networking and Application (PPNA) and Big Data Mining and Analytics (BDMA), he chaired over 30 international conferences. He is a Fellow of the British Computer Society (BCS).

Wenjing Lu works at the Affiliated Hospital of Jiangsu University, in Zhenjiang, the Jiangsu province, China. His main research interest has focused on pattern recognition and image processing.

Shenqi Jing works at the Jiangsu Province Hospital, in Nanjing, the Jiangsu province, China. His main research interests include big data mining and medical image processing.

Xiaoliang Zhang works at the Jiangsu Province Hospital, in Nanjing, the Jiangsu province, China. His main research interests include big data mining and medical image processing.

Xinxin Guo received his Ph.D. degree in management science and engineering from the Southeast University, Nanjing, China. He visited the Purdue University from September 2018 to September 2019 as a visiting scholar. He is currently a lecturer in the School of Management at the Jiangsu University. His research interests include mobile crowdsensing, data trading and healthcare service. He has published more than 10 papers in well-known journals and conferences.

Anna Shen works at the Affiliated Hospital of Jiangsu University, in Zhenjiang, the Jiangsu province, China. Her main research interests focus on pattern recognition and image processing.